Effects of atmospheric conditions on surface diffuse degassing

Antonio Pio Rinaldi, Jean Vandemeulebrouck, M. Todesco, Fatima Viveiros

Effects of atmospheric conditions on surface diffuse degassing

A. P. Rinaldi[1,2], J. Vandemeulebrouck[3], M. Todesco[1], F. Viveiros[4]

A. P. Rinaldi, Lawrence Berkeley National Laboratory, 1 Cyclotron Road, 94720 Berkeley, California, USA (aprinaldi@lbl.gov, antonio.rinaldi@bo.ingv.it)

M. Todesco, Istituto Nazionale di Geofisica e Vulcanologia, via Donato Creti, 12, 40128 Bologna, Italy. (micol.todesco@bo.ingv.it)

J. Vandemeulebrouck, ISTerre, CNRS, Université de Savoie, Campus Scientifique, 73376 Le Bourget du Lac Cedex, France. (Jean.Vandemeulebrouck@univ-savoie.fr)

F. Viveiros, Centro de Vulcanologia e Avaliação de Riscos Geológicos, Universidade dos Açores, Rua Mãe de Deus, Ponta Delgada, P9501801, Portugal. (Maria.FB.Viveiros@azores.gov.pt)

[1]Istituto Nazionale di Geofisica e

Abstract. Diffuse degassing and fumarolic activity are secondary manifestations of active volcanoes. Monitoring of these manifestations plays a key role in understanding the activity status of volcanoes, and the installation of permanent stations to measure the CO_2 flux at the surface are becoming more common. The measured gas fluxes often present a correlation with environmental observables, such as air temperature or barometric pressure, especially when gas emission is low. An example is the Furnas volcano (Azores), which features low temperature fumaroles, CO_2-rich springs, and several diffuse degassing areas. The hydrothermal CO_2 flux through the soil is continuously recorded by permanent gas stations coupled with several meteorological sensors. Daily and seasonal cycles have been observed in the time series of CO_2 flux. Air temperature and barometric pressure are the variables

Vulcanologia, Sezione di Bologna, Italy.

[2]Lawrence Berkeley National Laboratory,
Earth Sciences Division, Berkeley,
California, USA.

[3]ISTerre, CNRS, Université de Savoie,
Chambery, France.

[4]Centro de Vulcanologia e Avaliação de
Riscos Geológicos, Universidade dos Açores,
Portugal.

that best correlate with the CO_2 flux cycles. To understand the influence of atmospheric and soil conditions on the gas emission, several simulations with TOUGH2 simulator were performed. A simple 1D model was developed to understand the physical mechanisms producing the observed variations. Then, a dual parameters study focused on how rock permeability and gas source properties affect the resulting fluxes. Numerical results are in agreement with the observed data and show that changes in the barometric pressure and air temperature may cause changes in the observed CO_2 fluxes, which depend on rock permeability and on pressure driving the upward flux.

1. Introduction

Continuous measurements of carbon dioxide flux are now commonly used to monitor the degassing in volcanic environments [*Chiodini et al.*, 1998, 2010; *Hernández et al.*, 2001]. The transfer of the CO_2 to the surface results from two different physical processes, namely advection and diffusion [e.g. *Werner et al.*, 2000]. Advective transport is mainly induced by pressure gradient, and by temperature gradients that create density differences. Diffusion, on the other hand, is controlled by concentration gradients. For both advection and diffusion processes, the flux depends on the properties of the gas source, on the petrophysical properties of the soil, e.g. permeability, and on the conditions at the surface. In this paper, we aim at modeling how the periodic variations of air temperature and pressure at the soil surface can affect the CO_2 flux signals by producing harmonic variations at the same periods. A second goal is to understand if the monitoring of the periodic flux variations could be used to detect source or medium properties changes. Our model will be tested on CO_2 flux signal recorded at Furnas volcano (Azores, Portugal).

The impact of environmental variables on soil gas emissions has been studied in several degassing areas in the last decades [e.g. *Clements and Wilkening*, 1974; *Reimer*, 1980; *Klusman and Webster*, 1981; *Hinkle*, 1990, 1994; *Chiodini et al.*, 1998; *McGee and Gerlach*, 1998; *McGee et al.*, 2000; *Rogie et al.*, 2001; *Granieri et al.*, 2003, 2010; *Hernández et al.*, 2004; *Lewicki et al.*, 2007; *Viveiros et al.*, 2008, 2009; *Cigolini et al.*, 2009]. However very few papers were found in the literature that analyzed diurnal variations for the soil CO_2 flux in hydrothermal environments. *Chiodini et al.* [1998] noticed that CO_2 flux variations at Vulcano (Aeolian Islands, Italy) were affected by barometric pressure changes

rather than by absolute atmospheric pressure value. *Granieri et al.* [2003] identified a 24 h cycle in CO_2 fluxes from Solfatara volcano between 1998-2002 and *Padrón et al.* [2008] recognized diurnal and semidiurnal fluctuations in the gas flux acquired during 2004 in a station located at El Hierro (Canary Islands). On the other side, diurnal and seasonal variations of CO_2 flux derived from soil respiration (biogenic origin) have been intensely studied as CO_2 production is dependent on the temperature and the CO_2 oscillations are positively correlated with the air/soil temperature changes [*Witkamp*, 1969; *Bajracharya et al.*, 2000; *Nakadai et al.*, 2002], as well as with the wind speed [*Takle et al.*, 2004; *Reicosky et al.*, 2008; *Bowling and Massman*, 2011]. Biogenic fluxes are also influenced by atmospheric pressure [*Massman*, 2004]. These papers recorded the correlation but did not investigate the processes that cause and explain the observed trends.

Some studies have also recognized periodicities on ^{222}Rn time series in the air [e.g. *Rigby and La Pointe*, 1993; *Pinault and Baubron*, 1997; *Robinson et al.*, 1997; *Groves-Kirkby et al.*, 2006; *Steinitz et al.*, 2007; *Richon et al.*, 2009] and in the soil [*Aumento*, 2002; *Richon et al.*, 2003, 2011; *Cigolini et al.*, 2009]. For example, *Clements and Wilkening* [1974] observed that pressure variations of 1% - 2% changes the radon flux from 20% to 60%.

This work intends to understand the influence of atmospheric and soil conditions on the gas release, by performing several simulations with TOUGH2 geothermal simulator [*Pruess et al.*, 1999]. Although such a simulator is largely used in non-volcanological contests [e.g. *Oldenburg and Rinaldi*, 2011; *Borgia et al.*, 2012; *Mazzoldi et al.*, 2012], applications in volcanology are becoming more common for the study of diffuse degassing [e.g. *Todesco et al.*, 2010; *Chiodini et al.*, 2010] and of the geophysical and geochemi-

cal signals related to hydrothermal fluids circulation [e.g. *Hutnak et al.*, 2009; *Rinaldi et al.*, 2010, 2011]. We used the TOUGH2/EOS2 module to describe CO_2 in gas phase fluid. Using a 1D model, a parametric study was performed to understand the physical mechanisms producing the observed variations. Numerical results, in agreement with the observed data, show that the CO_2 fluxes are strongly dependent on reservoir pressure, temperature and pressure changes applied at the surface, and on domain permeability.

2. A case study: Influence of atmospheric conditions on the CO_2 degassing at Furnas volcano

Secondary manifestations of volcanism in the Azores archipelago (Fig. 1) include low temperature fumaroles (maximum temperature around 100 °C), hot and cold CO_2-rich springs, and several diffuse degassing areas. Continuous monitoring of hydrothermal soil CO_2 flux begun on Furnas volcano, S. Miguel island, in October 2001, with the installation of a permanent gas station that incorporates several meteorological sensors. Daily and seasonal cycles have been observed in the time series of soil CO_2 flux and are coincident with the periodical behavior of some meteorological parameters. Statistical analysis applied to the recorded time series shows that air temperature, barometric pressure, rainfall, and wind speed are the observables that better correlate with the soil CO_2 flux variations [*Viveiros et al.*, 2008, 2009]. These external parameters may also have a different effect on the gas flux depending on the characteristics of the monitoring site (e.g. physical properties of the soil, topographic effects, drainage area).

Two permanent soil CO_2 flux monitoring stations are presently installed inside Furnas volcano caldera (S. Miguel Island, Azores archipelago) (Fig. 1). *GFUR1* station, which was running between October 2001 and July 2006, was placed in a garden of the Furnas

thermal baths, close to Furnas village fumarolic field. Average values measured of CO_2 flux were ∼260 g m^{-2} d^{-1} and soil temperature was about 17 °C. The station was reinstalled (and renamed as *GFUR3*) in January 2008 closer to Furnas village main fumaroles, in a thermally anomalous zone where the average soil temperature is 38 °C at 30 cm depth, with a soil CO_2 flux ∼650 g m^{-2} d^{-1}. A soil CO_2 flux station (named *GFUR2*) was also installed inside Furnas caldera in the vicinity of Furnas Lake fumarolic ground in October 2004, where soil CO_2 flux values around 350 g m^{-2} d^{-1} were measured. Soil temperature at this site is ∼22 °C at about 30 cm of depth. According to *Viveiros et al.* [2010], the stations are all installed in diffuse degassing structures (DDS) that are fed by the hydrothermal sources.

The permanent flux stations perform measurements based on the accumulation chamber method [*Chiodini et al.*, 1998]. Every hour, a chamber is lowered on the ground and the gas released at the ground surface is pumped into an infrared gas analyzer (IRGA).

The soil CO_2 flux value is computed as the linear best fit of the flux curve during a predefined period of time. Measurements have a reproducibility within 10% for the CO_2 range between 10 and 20000 g m^{-2} d^{-1} [*Chiodini et al.*, 1998]. The gas flux automatic stations have also coupled meteorological sensors and acquire simultaneously the barometric pressure, air temperature, air relative humidity, wind speed and direction, rainfall, soil water content and soil temperature.

2.1. Spectral analysis applied to CO_2 flux data at GFUR2

Seasonal periodicities and diurnal variations are observed on the CO_2 time series concomitant with the periodicity observed in some meteorological variables (e.g. air temperature, air relative humidity, and barometric pressure). We choose to analyze data

registered at station GFUR2 during the summers of the whole period (2005 - 2009, from May to September), since, in that period of the year, average monthly rainfall is low, and then rainfall effects on degassing can be considered as negligible. In addition, GFUR2 is the monitoring site with longer register at Furnas volcano.

The magnitude of the diurnal variations on the soil CO_2 flux (usually from 50 to 100 g m^{-2} d^{-1}) excludes the possibility of a biogenic origin of the CO_2 variations. Works published in biogenic environments [e.g. *Nakadai et al.*, 2002] refer significantly lower daily amplitudes (about 5 - 6 g m^{-2} d^{-1}), indicating that the site of the present study at Furnas are clearly fed by volcanic-hydrothermal sources.

Diurnal and semi-diurnal components are observed in the soil CO_2 flux time series (Fig. 2), with 24h period peak significantly stronger than 12h period peak. Air temperature, air relative humidity, barometric pressure, and wind speed recorded at GFUR2 site show as well daily fluctuations. Figure 3 shows an example of a summer week variation of CO_2 flux, air temperature, and barometric pressure, observed at GFUR2. The diffuse emission of carbon dioxide reaches maximum values early in the morning, when atmospheric pressure and temperature are lower. The variations of the two atmospheric parameters will be used as an evolving, top boundary condition in the numerical simulation (see next section).

The correlation coefficient between the monitored variables and the time delays between them were calculated, for the 24h and 12h peaks. Only correlation coefficients higher than 0.5 were included in Table 1. For the 24 h component, the soil CO_2 presents the highest correlation ($r > 0.8$) with wind speed, air temperature, and air relative humidity. With respect to the 12h component, air temperature and wind speed are the meteorological variables that better correlate with the CO_2 flux ($r \sim 0.7$). We considered the wind as a

perturbation of lower period (less than 12 h), which means that its effect is very shallow, with a penetration up to some decimeters but with a large impact. *Viveiros et al.* [2008] recognized the inverse correlation between CO_2 flux and wind speed and suggested that during high wind speed events the soil gas is diluted with atmospheric air pushed into the upper parts of the soil. This correlation is potentially favored by the soil porosity and permeability. Barometric pressure shows in general a worse correlation with diffuse degassing, with the lowest coefficient found for the 24h component, but it better correlates with the soil degassing for the 12h component ($r \sim 0.7$). Table 1 also reports the time delay between the different atmospheric parameters and the two harmonic components of CO_2 flux. Air relative humidity shows no delay with respect to the diurnal component (24h period). Air temperature and wind speed show a 10 - 11 h delay with respect to the 24h component, and a 6h delay for the 12h component. The delay between barometric pressure and CO_2 flux is about 6h for the 24h component and 4h for the 12h component at GFUR2 monitoring site.

In our case, the CO_2 flux released by an hydrothermal area has an opposite behavior to that observed where CO_2 is entirely biogenic, and where the CO_2 oscillations are positively correlated with temperature changes [*Witkamp*, 1969; *Bajracharya et al.*, 2000; *Nakadai et al.*, 2002].

3. Numerical simulation

In order to compute the CO_2 flux changes that arise from variations in atmospheric pressure and temperature conditions and to understand the role played by rock permeability and reservoir overpressure on observed delay, parameter studies of fluid circulation were carried out with the TOUGH2/EOS2 simulator [*Pruess et al.*, 1999]. Briefly, TOUGH2 is

a multi-purpose simulator for fluids in porous medium. Using an integral finite difference method for mass and energy balance, and a first order finite difference for time discretization, fluids can be simulated as multi-phase and multi-component, taking into account both the effects of relative permeability of each phase and capillarity pressure. The module EOS2, here used to simulate the CO_2 flux only, may account for the presence of water and carbon dioxide. Heat transfer in TOUGH2 occurs both by conduction and convection, and it accounts for latent heat effects. A thermodynamic equilibrium is assumed to be present between fluids and porous matrix. We do not account for chemical reaction nor deformation of the rock matrix. At this time, we focus on the unsaturated, upper portion of the soil that we consider fully saturated with carbon dioxide. We are aware that the presence of liquid water may significantly alter the simulated CO_2 flux, but this effect is beyond the limits of the present work. The equations solved in TOUGH2/EOS2 for single-phase conditions and CO_2 as the only fluid component are shown in Table 2.

We aim to analyze the effects of the atmospheric conditions on diffuse degassing looking at diurnal and semi-diurnal variation of CO_2 flux, and for this reason we simulated a week-long variation of the air temperature and barometric pressure, modifying the boundary conditions at the top of the domain. The variations of the physical quantities correspond to data collected at the GFUR2 station (Fig. 3).

Figure 4 describes the 1D domain, 1 m deep, with the rock properties. The domain was discretized into 42 elements of 2.5 cm. Here we assume that the observed surface CO_2 flux is fed by a hydrothermal reservoir at depth, which is slightly hotter and pressurized with respect to atmospheric conditions. To represent such conditions, we assume that the bottom boundary of the domain (reservoir) is open to fluid flow, and has a fixed

temperature, 3 °C above the initial atmospheric temperature ($T_{\mathrm{atm}} = 17.23$ °C), and fixed reservoir pressure, which is higher than initial atmospheric pressure ($p_{\mathrm{atm}} = 0.09927$ MPa). Temperature gradient follows observations at Furnas monitoring site, although changes in the initial temperature distribution do not affect the results (see next section). The choice of reservoir pressure (and hence the overpressure Δp that drives the flow) depends on the considered simulation. The top boundary is open and at prescribed atmospheric pressure and temperature, which both change according to the observed temporal variations.

Initial conditions correspond to a steady state that was reached with a long simulation (hundreds of year), which produced a linear pressure and temperature gradients in the medium.

3.1. Furnas case

We first present a detailed analysis of a base case, in order to describe which mechanisms drive and affect the degassing. Rock properties and bottom boundaries conditions for this base case were chosen to match the CO_2 flow variation observed at GFUR2 during the considered week (Fig. 3). We chose a domain permeability $\kappa = 2{\cdot}10^{-14}$ m^2 and an overpressure in the reservoir $\Delta p = 0.05$ MPa, with respect to the initial atmospheric pressure. At steady state conditions, the system is characterized by temperature and pore pressure linear gradients, and by a stationary upward CO_2 flow. Starting from these conditions, we run a week-long simulation, imposing the observed variations of atmospheric pressure and temperature along the top boundary.

Figure 5 shows the results of the simulation on the week-long record. The simulated CO_2 flux (blue line) changes when the perturbation is applied to the surface and tends to

be inversely correlated to both air temperature (red line) and pressure (black line). The simulated flux presents a large diurnal change, reflecting the effect of the temperature time series. A longer-period variation, about 3 days long, also appears in the simulated CO_2 flux, and is associated with atmospheric pressure changes, with the same period of variation. Gas flux also displays a semi-diurnal component, induced by atmospheric pressure changes, but of smaller amplitude. This pressure-induced effect can be clearly seen around the hour 20, where the linear temperature change cannot be responsible of the 12h-period change.

Results of modeled CO_2 flux at the surface obtained with the chosen permeability and gas reservoir overpressure are in good agreement with the changes observed at GFUR2 (Fig. 5b). Some discrepancy may result from the fact that we do not take into account effects of wind, air humidity, and soil water content.

The effects of the evolving boundary conditions are not confined to the ground surface, but propagate downward, causing changes of the CO_2 flux throughout the domain (Fig. 5c). The CO_2 flux observed at the base of the domain presents almost the same variation of the degassing simulated at ground surface.

The applied pressure and temperature perturbations propagate over the 1 m-high domain (Fig. 6a,b,c,d). Applied atmospheric pressure changes are of the order of few hundreds Pa, and this pressure perturbation often reaches most of the computational domain (Fig. 6b). However, these changes are small compared to the average pressure within the system (order of 10^5 Pa). Although the initial pressure distribution is mostly unaffected (Fig. 6a), the changes in the atmospheric pressure clearly influence the simulated CO_2 flux. On the other hand, the changes of air temperature (Fig. 6d) are larger compared

to the average temperature of the whole system, and clearly alter the initial temperature distribution (Fig. 6c). Both pressure and temperature perturbations cause changes of gas density (Fig. 6e,f).

4. Comparison between harmonic flux changes in model and observations

4.1. Power spectra

In order to understand which atmospheric perturbation has the largest effect on the resulting CO_2 degassing, a spectral analysis has been performed. When a perturbation of a certain period generates large variations in the resulting time series, then the data will show a large peak in the spectrum at that particular period.

Using as example the Furnas case analyzed in the previous section, we now analyze the power spectrum of the gas flux time series to find out its characteristic frequencies. In order to focus on the diurnal and semi-diurnal components, we low-pass filtered the data of the week-long record, and keep only periods lower than 28 h (Fig. 7). Without longer periods, the pressure has a main 12h period, with a very small component at 24h. The temperature is only slightly affected by the filter, since it is mainly characterized by periods shorter than 24h. Temperature has a main peak at 24h, and a twenty-times smaller peak at 12h. The gas flux in this base case has a main 24h period, but the 12h component is strong enough to affect the temporal evolution. The ratio 12h peak/24h peak for the gas flux is about 7%, larger than the 5% we found for the temperature. This suggests that in this base case, the temperature variation mostly affect the evolution of gas flux (for the 24h period). A small variation in the 12h period is noticeable, and it is due to the application of the pressure perturbation, otherwise the ratio 12h peak/24h peak would have been the same for gas flux and temperature. The influence of pressure

can also be seen in the effect of long-term (several days) pressure changes, as during the studied week where pressure and CO_2 long-term changes are well correlated.

4.2. Time delay

The time delay between the applied perturbations (atmospheric pressure or temperature) and the resulting CO_2 flux time series may provide interesting information on the properties of the soil and on the conditions of the hydrothermal reservoir. We apply a band pass filter centered on the selected period (24h or 12h) with a 4 h bandwidth, in order to compare only the 24h component of the gas flux to the air temperature, and only the 12h component of the gas flux to the atmospheric pressure. It is of note that the 12h peak of the power spectrum is one order of magnitude below the 24h.

Results of the band-pass filtering of the simulated gas flux are shown in Figure 8 and compared with the filtered pressure (Fig. 8b) and temperature (Fig. 8c), respectively.

The time series are now very smooth and comparable, and it is quite easy to calculate a time delay as a time shift between the two series by a correlation method. For the base case simulation (normalized resulting gas flux and perturbations in Fig. 8a), results show a time delay of 6 hours when compared with the atmospheric pressure time series (Fig. 8b), and a time delay of 15.25 hours when compared with the temperature time series (Fig. 8c). Time delay may change when domain properties are changed (see next section), however, these results are in good agreement with the delays observed at Furnas (see Tab. 1). Note that the observed delay at Furnas were obtained by processing CO_2 flux data during several summers and not only during a week, as in our simulation study.

5. Effect of permeability and source pressure on 12h and 24h CO_2 flux components

In this section, a two parameters study will be presented. The changes in peak amplitude in the spectrum and time delay of the 24h and 12h components of the flux variations will be analyzed as a function of the rock permeability and the gas reservoir overpressure. Domain permeability ranges between 10^{-15} m^2 and 10^{-11} m^2, and gas reservoir overpressure between $2{\cdot}10^{-5}$ and 0.1 MPa.

The first set of simulations was run changing the rock permeability and keeping a constant gas reservoir overpressure as in the base case (0.05 MPa, a value that is consistent with observed gas flux). The resulting changes in peak amplitude and time delay are shown in Figure 9. The peak amplitude of the simulated CO_2 flux always presents both the 12h and 24h component (Fig. 9a, green and blue lines, respectively). However, the two analyzed components are not always comparable. The 24h component is dominant for most of the considered permeabilities. More than one order of magnitude differences between 24h and 12h components appear for low permeabilities. This difference decreases at higher permeability, and the two considered components have the same order of magnitude for the highest permeability considered (10^{-11} m^2). Results also show changes in time delay (Fig. 9b). The 24h component of the CO_2 flux has a delay with respect the temperature perturbation ranging between 18 hours and 14 hours (Fig. 9b, blue line). The higher the permeability, the lower the delay observed. The delay of the 12 h component of the CO_2 flux with respect to the pressure perturbation is rather constant ($\sim$ 6 hours) for most of the simulated permeabilities, and increases up to 8 hours only for permeability lower than 10^{-14} m^2 (Fig. 9b, green line).

The second set of simulations was run keeping a constant rock permeability, set as in the base case ($2{\cdot}10^{-14}$ m^2), and changing the overpressure at the base of the domain. Figure 10 shows the changes in peak amplitude and time delay as a function of the gas reservoir overpressure. Again, all the simulated cases present both the 12h and 24h components. The peak amplitude for the 12 h component of the CO_2 flux has a constant value for low overpressure (up to 0.01 MPa), then it exponentially decreases for higher overpressure (Fig. 10a, green line). The 24h component features an opposite behavior: it starts to increase exponentially for overpressure greater than few thousands Pa (Fig. 10a, blue line). The ratio between the peak amplitudes of the two considered components reaches a maximum of three orders of magnitude for the highest simulated overpressure. This means that for low overpressure the system seems to have only a 12h component, which indicates that it is only affected by pressure perturbations. At higher overpressures, the CO_2 flux appears to have only a 24h component, which means that only the temperature perturbation affects the resulting degassing. The time delay only slightly changes as a function of the gas reservoir overpressure. The 12h component has a constant delay of $\sim$6 hours with respect to the pressure for all the considered overpressure (Fig. 10b, green line). The time delay of the 24h component with respect to the temperature is larger than 18 hours for low overpressure, and starts to decrease when the overpressure is greater than one thousand Pa, up to a minimum, constant value of $\sim$15 hours for the highest overpressures simulated (0.05 – 0.1 MPa) (Fig. 10b, blue line).

Figure 11 shows a dual parameters analysis of the time delay and peak amplitude in the spectrum. Throughout the studied parameters domain, the 12h component of the CO_2 flux presents a stable delay around 6 hours with respect the barometric pressure (Fig.

11a), and reaches a maximum of 8 hours only for very low permeability (10^{-15} m^2). The delay of the 24h component with respect the atmospheric temperature is shown in Figure 11b. This delay remarkably changes in the parameters space: a high delay ($\sim$ 21 hours) is observed for low permeability and low gas reservoir overpressure. Then, this time delay lowers when both permeability and gas reservoir overpressure increase, the minimum value ($\sim$ 13 hours) being observed for the highest gas reservoir overpressure (0.1 MPa) and rock permeability (10^{-11} m^2) simulated. It is interesting to note that the time delay is more sensitive to rock permeability at low reservoir overpressures. Contrarily, at very high permeability, changes in the gas reservoir overpressure only cause slight changes of the time delay.

Figures 11c and d show the amplitude of the peak in the spectrum for the 12h and 24h components of the simulated CO_2 flux as a function of both rock permeability and gas reservoir overpressure. Some elements of discussion can arise from the comparison between these two figures. In the range of the simulated permeabilities and gas reservoir overpressure, it seems that the CO_2 flux has a 24h component larger than the 12h component, i.e. once again the temperature perturbation seems to be more effective on the simulated degassing. However, there are some regions in the parameters space where the peak amplitude of the 12h component is slightly higher than, or at least comparable with the peak amplitude of the 24h component. This happens for small gas reservoir overpressure (up to 0.01 MPa) and for permeabilities in the range 10^{-14} – 10^{-11} m^2. Moreover, the peak amplitudes of the two considered components are comparable for very high permeabilities ($\sim 10^{-11}$ m^2). In the 12h peak amplitude diagram (Fig. 11c), the iso-amplitude lines are parallel to the overpressure axis, and indicate that this amplitude

is mainly influenced by permeability rather than source pressure changes. A similar, but less marked, pattern is observed in Figure 11d for the amplitude of the 24h component.

Analyzing the changes in 24h and 12h peak in the spectrum, a change in soil permeability will provoke a remarkable and similar increase of both 12h and 24h components, while an increase in the gas reservoir overpressure will induce a different behavior of the two components, with the 24h component increasing while the 12h component decreases (or remains constant). Thus the observation of a correlated change in the 12h and 24h peak amplitudes of the gas flux spectrum may suggest a permeability change in the soil, rather than a change in source conditions as a driving mechanism. It is of note that for low permeabilities, the evolution of the 12h component time delay can also help to distinguish a permeability change from a pressure change.

The described trend could be affected by our choice of initial conditions. The simulations described above were all run with an initial low temperature gradient (3 °C/m). Additional simulations were performed to asses the role of the initial temperature distribution. Results, shown in Figure 12, suggest that the initial temperature gradient does not affect (or slightly affects) the resulting CO_2 flux. The peak amplitude of both 12h and 24h components is constant in the range 3–30 °C/m (Fig. 12a), and the same is observed for the time delay for both components (Fig. 12b).

6. Discussion and Conclusion

This work focused on the effects of the atmospheric conditions on soil diffuse degassing. Harmonic oscillations are observed on the soil CO_2 flux time series at Furnas volcano in S. Miguel island in the Azores archipelago, and these variations are correlated with

the meteorological variables monitored by permanent stations (wind velocity, barometric pressure and air temperature).

Numerical results performed with the TOUGH2/EOS2 simulator show that the CO_2 flux changes when air temperature and barometric pressure change, and presents a time delay with respect to the applied perturbations in agreement with data observed at Furnas. The simulated degassing presents both diurnal and semi-diurnal variations, as effects of applied temperature and pressure, respectively. Lower fluxes are observed when temperature and pressure are higher, in agreement with data from Furnas, where lower degassing is observed during the afternoon.

The variable conditions imposed along the upper boundary of the domain affect the gas flux acting on the terms of the Darcy's flow equation: the pressure gradient and the fluid properties. Air temperature acts on fluid mobility (i.e. the ρ/μ term, see Tab. 2): lower temperatures correspond to higher CO_2 density values and lower viscosity. Since the gas flow is directly proportional to its density and inversely proportional to its viscosity (eq. 4 in Tab. 2), a temperature drop has the overall effect of increasing the fluid flow, and viceversa. The gas density also enters in the buoyancy term in the Darcy's flow equation ($\nabla P - \rho \mathbf{g}$). As we are dealing with uprising fluids, in this case higher density hinders the upward motion of the fluid. However, under the conditions considered here, the gas density is very small (on the order of 2 kg/m ^{3}) and this term is negligible with respect to the pressure gradient (the pressure difference across the domain is of the order of a few thousands Pa).

The atmospheric pressure acts in different and opposite ways. On one hand, it controls the pressure gradient. In our degassing system, the pore pressure at depth is larger than

at the top. If the atmospheric pressure further diminishes, the gradient across the surface increases, leading to a higher gas flux. Pressure also acts on the CO_2 density, which in this case is directly proportional to it. A high atmospheric pressure act on gas flux reducing the pressure gradient, but increasing the contribution due to density.

The overall value of the gas flux at the surface depends on the complex interplay of all these different contributions, and on their relative magnitude. Under the conditions considered here, the largest changes in the simulated gas flux are associated with the changes of CO_2 mobility, which is mostly controlled by temperature. Pressure effects arise through the pressure gradient term, but affect the degassing to a smaller extent. In this particular case, temperature and pressure are both inversely proportional to gas flux, and their effects can sum up at particular times, when they both follow similar increasing or declining trends.

Applied perturbations and simulated gas flow changes are not only confined at the ground surface, but propagate down to the bottom of the simulated domain. This effect is mainly controlled by the chosen domain permeability and gas reservoir overpressure. The perturbation applied at the surface as described above may be balanced before reaching the reservoir at depth when the fluid flow is slow (as in the case of very low permeability), or affect only the upper part of the domain when the pressure changes applied at the surface are of the same order of magnitude or greater than the overpressure imposed at the reservoir.

Degassing may be affected by many parameters, among which rainfall, air humidity, and wind speed, and then it is not possible to directly compare the absolute values of simulated and observed CO_2 flux. However, results for a base case show a variation in degassing of

399 the same order of magnitude of the observed changes at Furnas. We calculated two time
400 delays: the correlation between the 24h component of the CO_2 flux with respect the air
401 temperature, and between the 12h component of the gas flux with respect the barometric
402 pressure. Results highlight a delay of $\sim$ 15 hours for the 24h component, and a delay of
403 $\sim$ 6 hours for the 12h component, well in agreement with what observed in the real field,
404 although, even in this case, time delays may be affected by other perturbations.

405 CO_2 flux time series depend on both the domain permeability and the overpressure
406 in the gas reservoir. In order to understand the role played by the rock permeability
407 and by an overpressure driving gas ascent, a dual parameters study was performed. The
408 dual parameters study highlights changes in time delay and peak amplitude for both the
409 considered components of the CO_2 flux (12h and 24h).

410 Analyzing the time delay, on one hand a mostly constant delay around 6 hours results
411 for the 12h component, and this delay slightly changes only for very low permeabilities
412 (up to 8 hours); on the other hand the delay for the 24h component presents remarkable
413 changes, ranging from 13 hours for high permeability and overpressure, to 21 hours when
414 both the rock permeability and the gas reservoir overpressure are low.

415 Amplitude of the peak in the spectrum for both components also changes as a function of
416 rock permeability and gas reservoir overpressure. This study highlights how the CO_2 flux
417 main period depends on the system properties. From the analysis of the peak amplitude,
418 the resulting degassing has mainly a 12h period for low gas reservoir overpressure (up to
419 0.01 MPa) and for permeability higher than 10^{-14} m^2. The peak amplitude for the two
420 components are comparable for very high permeabilities, and the resulting degassing will
421 present in that case both the 12h and the 24h period.

These results indicate that a coupled analysis of these observables may provide useful hints to discriminate the parameter that is changing within the system. According to our model, the observation of correlated changes in the diurnal and semi-diurnal components of diffuse degassing, under the conditions described above, would be related to a permeability change in the soil. On the contrary, an unrelated evolution of these components would indicate a change in the source conditions. This is in agreement with the observations of *Richon et al.* [2003] that correlated changes in the 12h cycle of Rn time series with a magnitude 7.1 earthquake close to Taal volcano (Philippines). Permeability changes in a volcano/hydrothermal system can be generated by transient stresses, including distant earthquakes [*Elkhoury et al.*, 2006; *Manga et al.*, 2012], or may result from micro-fracturing associated with intrusive processes and mechanical disturbances, such as a dome collapse, or from mineral dissolution or precipitation [*White and Mroczek*, 1998]. The monitoring of harmonic components of the gas flux signal should thus be integrated in volcano monitoring as it represents a tool to understand the reasons of gas flux changes at the surface.

Acknowledgments. This work was carried out when the first author was enrolled in the Doctorate school at the University of Bologna, on a grant funded by the Istituto Nazionale di Geofisica e Vulcanologia - Sezione di Bologna. A. P. Rinaldi is currently supported by DOE-LBNL contract number DE-AC02-05CH11231. F. Viveiros is supported by a Postdoc grant from Fundo Regional da Ciência e Tecnologia.

References

Aumento, F. (2002), Radon tides on an active volcanic island: Terceira, Azores, *Geof. Int.*, *41*(4), 499–505.

Bajracharya, R. M., R. Lal, and J. N. Kimble (2000), Diurnal and seasonal CO_2-C flux from soil as related to erosion phases in central Ohio, *Soil Sci. Soc. Am. J.*, *64*, 286–293.

Borgia, A., K. Pruess, T. J. Kneafsey, C. M. Oldenburg, and L. Pan (2012), Numerical simulation of salt precipitation in the fractures of a CO_2-enhanced geothermal system, *Geothermics*, *44*, 13–22, doi:10.1016/j.geothermics.2012.06.002.

Bowling, D. R., and W. J. Massman (2011), Persistent wind-induced enhancement of diffuse CO_2 transport in a mountain forest snowpeak, *J. Geophys. Res.*, *116*, G04006.

Chiodini, G., R. Cioni, M. Guidi, B. Raco, and L. Marini (1998), Soil CO_2 flux measurements in volcanic and geothermal areas, *Appl. Geochem.*, *13*, 543 – 552.

Chiodini, G., S. Caliro, C. Cardellini, D. Granieri, R. Avino, A. Baldini, M. Donnini, and C. Minopoli (2010), Long term variations of the Campi Flegrei (Italy) volcanic system as revealed by the monitoring of hydrothermal activity, *J. Geophys. Res.*, *115*, B03205, doi:10.1029/2008JB006258.

Cigolini, C., et al. (2009), Radon surveys and real-time monitoring at Stromboli volcano: Influence of soil temperature, atmospheric pressure and tidal forces on ^{222}Rn degassing, *J. Volcanol. Geotherm. Res.*, *184*, 381–388.

Clements, W. E., and M. H. Wilkening (1974), Atmospheric pressure effects on ^{222}Rn transport across the Earth-Air interface, *J. Geophys. Res.*, *79*(33), 5025–5029.

Elkhoury, J. E., E. E. Brodsky, and D. C. Agnew (2006), Seismic waves increase permeability, *Nature*, *441*, 1135–1138, doi:10.1038/nature04798.

Granieri, D., G. Chiodini, W. Marzocchi, and R. Avino (2003), Continuous monitoring of CO_2 soil diffuse degassing at Phlegrean Fields (Italy): influence of environmental and volcanic parameters, *Earth Planet. Sci. Lett.*, *212*, 167–179.

Granieri, D., R. Avino, and G. Chiodini (2010), Carbon dioxide diffuse emission from the soil: ten years of observations at Vesuvio and Campi Flegrei (Pozzuoli), and linkages with volcanic activity, *Bull. Volcanol.*, *72*, 103–118, doi:10.1007/s00445-009-0304-8.

Groves-Kirkby, C. J., A. R. Denman, R. G. M. Crockett, P. S. Phillips, and G. K. Gillmore (2006), Identification of tidal and climatic influences within domestic radon time-series from Northamptonshire, UK, *Sci. Total Environ.*, *367*, 191–202.

Hernández, P., N. Pérez, J. Salazar, M. Reimer, K. Notsu, and H. Wakita (2004), Radon and helium in soil gases at Canãdas Caldera, Tenerife, Canary Islands, Spain, *J. Volcanol. Geotherm. Res.*, *131*, 59–76.

Hernández, P. A., et al. (2001), Carbon Dioxide Degassing by Advective Flow from Usu Volcano, Japan, *Science*, *292*, 83, doi:10.1126/science.1058450.

Hinkle, M. E. (1990), Factors affecting concentrations of helium and carbon dioxide in soil gases, in *Geochemistry of gaseous elements and compounds*, edited by E. M. Durrance, E. M. Galimov, M. E. Hinkle, G. M. Reimer, R. Sugisaki, and S. S. Augustithis, pp. 421–448, Theophrastus Publications, S. A.

Hinkle, M. E. (1994), Environmental conditions affecting He, CO_2, O_2, and N_2 in soil gases, *Appl. Geochem.*, *9*, 53–63.

Hutnak, M., S. Hurwitz, S. E. Ingebritsen, and P. A. Hsieh (2009), Numerical models of caldera deformation: Effects of multiphase and multicomponent hydrothermal fluid flow, *J. Geophys. Res.*, *114*, B04411, doi:10.1029/2008JB006151.

Klusman, R. W., and J. D. Webster (1981), Preliminary analysis of meteorological and seasonal influences on crustal gas emission relevant to earth prediction, *Bull. Seism. Soc. Am.*, *71*(1), 211–222.

Lewicki, J. L., G. E. Hilley, T. Tosha, R. Aoyagi, K. Yamamoto, and S. M. Benson (2007), Dynamic coupling of volcanic CO_2 flow and wind at the Horseshoe Lake tree kill, Mammoth Mountain, California, *Geophys. Res. Lett.*, *34*, L03401, doi: 10.1029/2006GL028848.

Manga, M., I. Beresnev, E. E. Brodsky, J. E. Elkhoury, D. Elsworth, S. E. Ingebritsen, D. C. Mays, and C.-Y. Wang (2012), Changes in permeability caused by transient stresses: Field observations, experiments, and mechanisms, *Re. Geophys.*, *50*, RG2004, doi:10.1029/2011RG000382.

Massman, W. J. (2004), Advective transport of CO_2 in permeable media induced by atmospheric pressure fluctuations: 1. An analytical model, *J. Geophys. Res.*, *111*, G03004.

Mazzoldi, A., A. P. Rinaldi, A. Borgia, and J. Rutqvist (2012), Induced seismicity within GCS projects: maximum earthquake magnitude and leakage potential from undetected faults, *Int. J. Greenhouse Gas Control*, submitted.

McGee, K. A., and T. M. Gerlach (1998), Annual cycle of magmatic CO_2 in a tree-kill soil at Mammoth Mountain, California: Implications for soil acidification, *Geology*, *26*(5), 463–466.

McGee, K. A., T. M. Gerlach, R. Kessler, and M. P. Doukas (2000), Geochemical evidence for a magmatic CO_2 degassing event at Mommoth Mountain, California, September-October 1997, *J. Geophys. Res.*, *105*, 8447–8456.

Nakadai, T., M. Yokozawa, H. Ikeda, and H. Koizumi (2002), Diurnal changes of carbon dioxide flux from bare soil in agricultural field in Japan, *App. Soil Ecol.*, *19*, 161–171.

Oldenburg, C. M., and A. P. Rinaldi (2011), Buoyancy Effects on Upward Brine Displacement Caused by CO_2 Injection, *Transp. Porous Med.*, *87*, 525 – 540, doi:10.1007/s11242-010-9699-0.

Padrón, E., P. A. Hernández, T. Toulkeridis, N. M. Pérez, R. Marrero, F. Melián, G. Virgili, and K. Notsu (2008), Diffuse CO_2 emission rate from Pululahua and the lake-filled Cuicocha calderas, Ecuador, *J. Volcanol. Geotherm. Res.*, *176*, 163–169.

Pinault, J. L., and J. C. Baubron (1997), Signal processing of diurnal and semidiurnal variations in radon and atmospheric pressure: A new tool for accurate in situ measurement of soil gas velocity, pressure gradient, and tourtuosity., *J. Geophys. Res.*, *102*(B8), 18,101–18,120.

Pruess, K., C. M. Oldenburg, and G. Moridis (1999), TOUGH2 user's guide, version 2.0, *Paper LBNL-43134.*, Lawrence Berkeley Natl. Lab., Berkeley, CA, USA.

Reicosky, D. C., R. W. Gesch, S. W. Wagner, R. A. Gilbert, C. D. Wente, and D. R. Morris (2008), Tillage and wind effects on soil CO_2 concentrations in muck soils, *Soil & Tillage Research*, *99*, 221–231.

Reimer, G. M. (1980), Use of Soil-Gas Helium Concentrations for Earthquake prediction: Limitations Imposed by Diurnal Variation, *J. Geophys. Res.*, *85*(B6), 3107–3115, doi:10.1029/JB085iB06p03107.

Richon, P., J. C. Sabroux, M. Halbwachs, J. Vandemeulebrouck, N. Poussielgue, J. Tabbagh, and R. Punongbayan (2003), Radon anomaly in the soil of Taal volcano, the Philippines: A likely precursor of the M7.1 Mindoro earthquake (1994)., *Geophys. Res.*

Lett., *30*(9), 1481, doi:10.1029/2003GL016902.

Richon, P., F. Perrier, E. Pili, and J. C. Sabroux (2009), Detectability and significance of 12 hr barometric tide in radon-222 signal, dripwater flow rate, air temperature and carbon dioxide concentration in an underground tunnel, *Geophys. J. Int.*, *176*, 683–694, doi:10.1111/j.1365-246X.2008.04000.x.

Richon, P., F. Perrier, B. P. Koirala, F. Girault, M. Bhattarai, and S. N. Sapkota (2011), Temporal signatures of advective versus diffusive radon transport at a geothermal zone in Central Nepal, *J. Environ. Radioactivity*, *102*(2), 88 – 102, doi: 10.1016/j.jenvrad.2010.10.005.

Rigby, J. G., and D. D. La Pointe (1993), Wind and barometric pressure effects on Radon in two mitigated houses, *The 1993 International Radon Conference*, pp. 61–68.

Rinaldi, A. P., M. Todesco, and M. Bonafede (2010), Hydrothermal instability and ground displacement at the Campi Flegrei caldera, *Phys. Earth Planet. Int.*, *178*, 155–161, doi: 10.1016/j.pepi.2009.09.005.

Rinaldi, A. P., M. Todesco, J. Vandemeulebrouck, A. Revil, and M. Bonafede (2011), Electrical conductivity, ground displacement, gravity changes, and gas flow at Solfatara crater (Campi Flegrei caldera, Italy): results from numerical modeling, *J. Volcanol. Geotherm. Res.*, *207*, 93 – 105, doi:10.1016/j.jvolgeores.2011.07.008.

Robinson, A. L., R. G. Sextro, and W. J. Riley (1997), Soil-gas entry into houses driven by atmospheric pressure fluctuations - The influence of soil properties, *Atmos. Environ.*, *31*(10), 1487–1495.

Rogie, J. D., D. M. Kerrick, M. L. Sorey, G. Chiodini, and D. L. Galloway (2001), Dynamics of carbon dioxide emission at Mammoth Mountain, California, *Earth Planet.*

Sci. Lett., *188*, 535–541.

Steinitz, G., O. Piatibratova, and S. M. Barbosa (2007), Annual cycle of magmatic CO_2 in a tree-kill soil at Mammoth Mountain, California: Implications for soil acidification, *J. Geophys. Res.*, *112*, B10211, doi:10.1029/2006JB004817.

Takle, E. S., W. J. Massman, J. R. Brandle, R. A. Schmiat, X. Zhou, I. V. Litvina, R. Garcia, G. Doyle, and C. W. Rice (2004), Influence of high-frequency ambient pressure pumping on carbon dioxide efflux from soil, *Agric. Forest Meteor.*, *124*, 193–206.

Todesco, M., A. P. Rinaldi, and M. Bonafede (2010), Modeling of unrest signals in heterogeneous hydrothermal systems, *J. Geophys. Res.*, *115*, B09213, doi: 10.1029/2010JB007474.

Viveiros, F., T. Ferreira, J. Cabral Vieira, C. Silva, and J. L. Gaspar (2008), Environmental influences on soil CO_2 degassing at Furnas and Fogo volcanoes (São Miguel Island, Azores archipelago), *J. Volcanol. Geotherm. Res.*, *177*, 883–893.

Viveiros, F., T. Ferreira, C. Silva, and J. L. Gaspar (2009), Meteorological factors controlling soil gases and indoor CO_2 concentration: a permanent risk in degassing areas, *Sci. Total Environ.*, *407*, 1362–1372.

Viveiros, F., C. Cardellini, T. Ferreira, S. Caliro, G. Chiodini, and C. Silva (2010), Soil CO_2 emissions at Furnas volcano, São Miguel Island, Azores archipelago: Volcano monitoring perspectives, geomorphologic studies, and land use planning application, *J. Geophys. Res.*, *115*, B12208, doi:10.1029/2010JB007555.

Werner, C., S. L. Brantley, and K. Boomer (2000), CO_2 emission related to the Yellowstone volcanic system 2. Statistical sampling, total degassing, and transport mechanisms, *J. Geophys. Res*, *105*(B5), 10,831 – 10,846.

White, S. P., and E. K. Mroczek (1998), Permeability Changes During the Evolution of a Geothermal Field Due to the Dissolution and Precipitation of Quartz, *Trans. Porous Med.*, *33*, 81–101, doi:10.1023/A:1006541526010.

Witkamp, M. (1969), Environmental effects on microbial turnover of some mineral elements: Part II–Biotic factors, *Soil Biol. Biochem.*, *1*(3), 177 – 184, doi:10.1016/0038-0717(69)90017-0.

Table 1. Correlation and time delay between each of the meteorological variables and the soil CO_2 flux at GFUR2 for the summer period.

	Corr. (r)		Delay (h)	
	24h comp.	12h comp.	24h comp.	12h comp.
Air humidity	0.880	0.686	0 h	0 h
Air temperature	0.890	0.721	11 h	∼6 h
Barometric pressure	0.533	0.683	∼6 h	∼4 h
Wind speed	0.904	0.727	10 h	∼6 h

Table 2. Governing equations solved in TOUGH2/EOS2 for single-phase, single-component (CO_2) non-isothermal cases. Symbols: V volume (m^3), M mass accumulation term (kg m^{-3}), Γ surface area (m^2), $\mathbf{F}$ Darcy flux vector (kg m^2 s^{-1}), $\mathbf{n}$ outward unit normal vector, q_V volumetric source term (kg m^{-3} s^{-1}), ϕ porosity, ρ and ρ_R fluid and rock density (kg m^{-3}), C_R heat capacity of the rock formation (J kg^{-1} K^{-1}), T temperature, u_{CO_2} internal energy (J kg^{-1}), κ permeability (m^2), μ dynamic viscosity (kg m^{-1} s^{-1}), P total pressure (Pa), λ thermal conductivity (J s^{-1} m^{-1} K^{-1}), h_{CO_2} enthalpy (J kg^{-1}). Equations are generally solved for each component and the heat "component". In this case we only consider a component, then the heat is considered as second component (superscript 2)

Description	Equation
Conservation of mass and energy	$\frac{\mathrm{d}}{\mathrm{dt}} \int_{V_n} M \,\mathrm{dV} = \int_{\Gamma_n} \mathbf{F} \cdot \mathbf{n} \mathrm{d}\Gamma + \int_{V_n} q_V \mathrm{dV}$
Mass accumulation	$M = \phi\rho$
Thermal energy accumulation	$M^{(2)} = (1-\phi)\rho_R C_R T + \phi\rho u_{CO_2}$
Phase flux	$\mathbf{F} = -\kappa\frac{\rho}{\mu}(\nabla P - \rho\mathbf{g})$
Thermal energy flux	$\mathbf{F}^{(2)} = -\lambda\nabla T + h_{CO_2}\mathbf{F}$

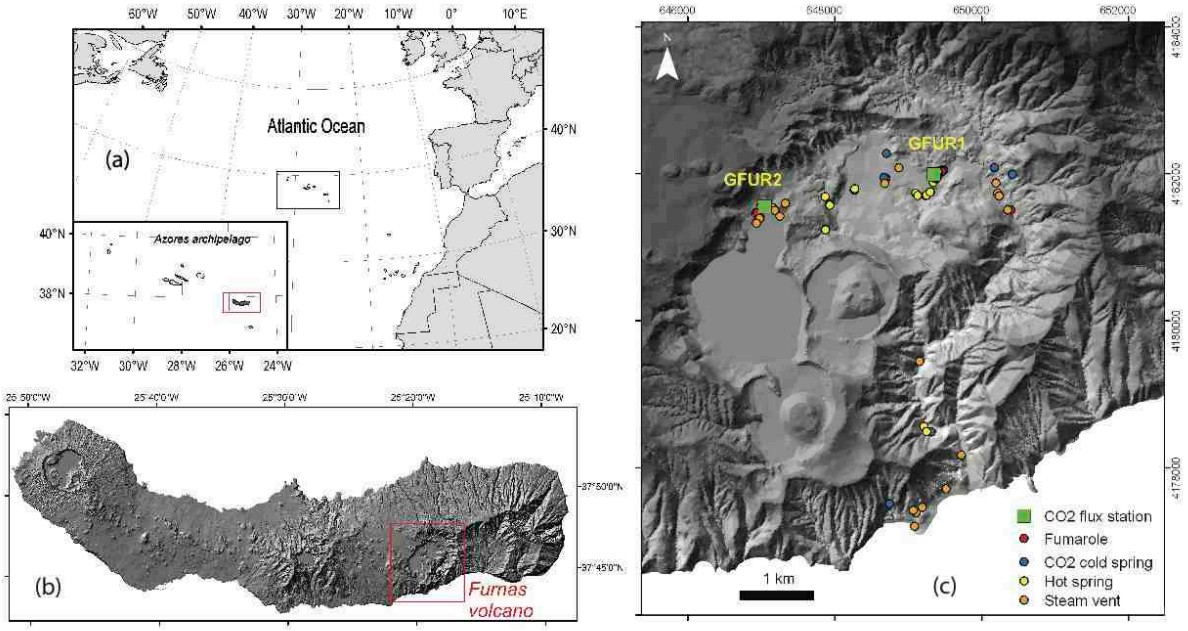

Figure 1. **(a)** Azores archipelago location highlighting S. Miguel Island; **(b)** Digital Elevation Model of the S. Miguel Island; (**c**) Hydrothermal manifestations and location of the permanent soil CO_2 stations at Furnas volcano.

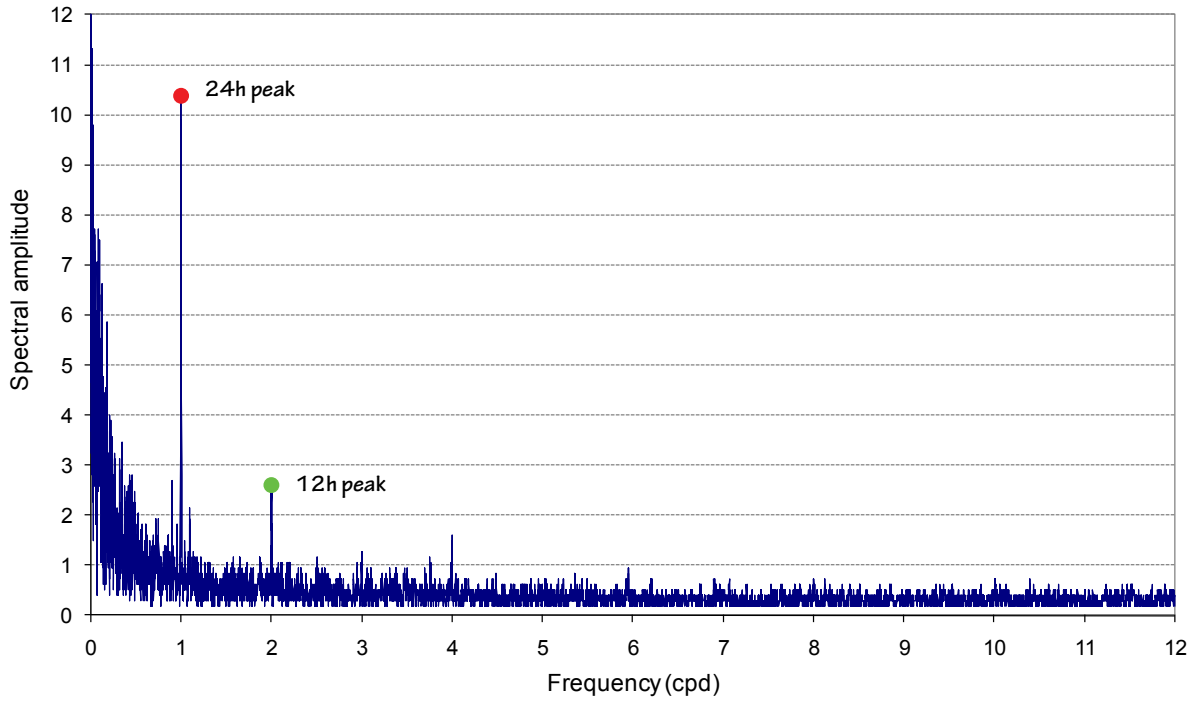

Figure 2. Amplitude spectrum of the soil CO_2 flux recorded at GFUR2 during summer months (2005-2009, from May to September). Red dot indicates the 24h peak (1 cpd). Green dot indicates the 12h peak (2 cpd). (cpd=cycles per day)

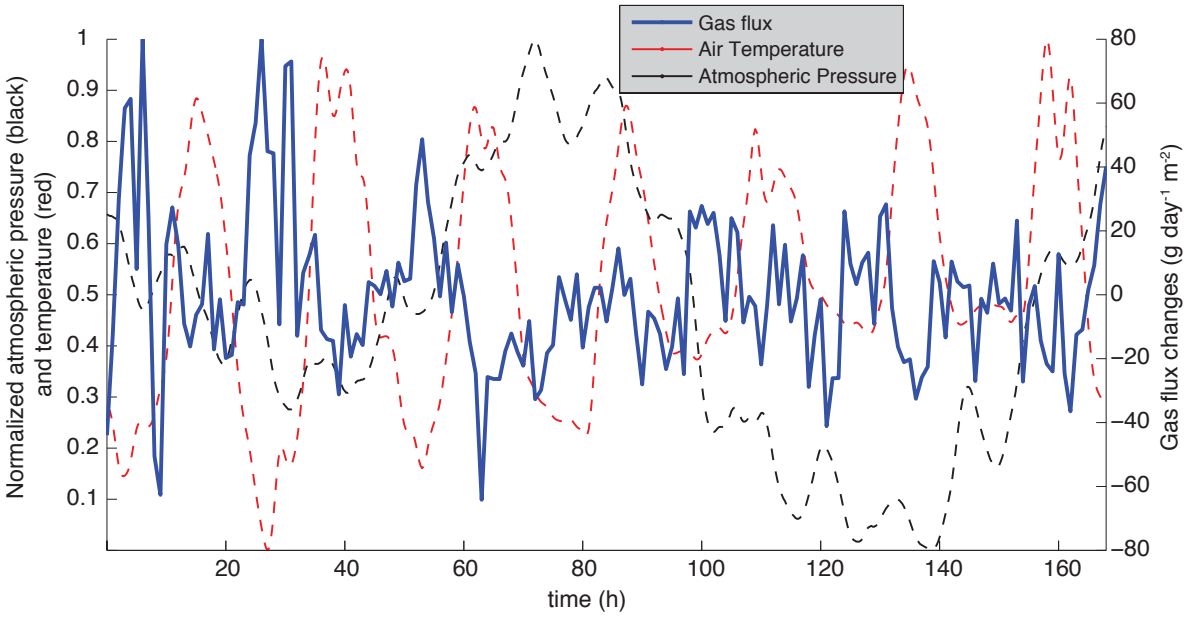

Figure 3. Example of atmospheric and CO_2 flux signals observed at GFUR2 station in a week of summer (7/9/2005-7/15/2005): air temperature (red, dashed), barometric pressure (black, dashed), and variations around the average CO_2 flux (blue, solid). Temperature and pressure are normalized in this figure.

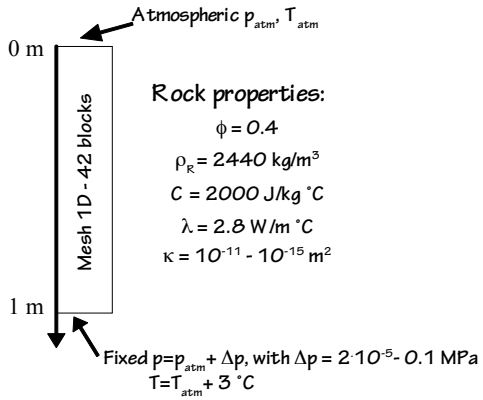

Figure 4. Numerical 1D domain and rock properties. ϕ is the porosity, ρ_R is the rock density, C is the specific heat, and λ is the thermal conductivity. These properties were kept constant during all the simulations. κ is the range of variation for the rock permeability. Atmospheric pressure and temperature depend on the considered simulation. For steady-state, initial conditions are $T_{\rm atm}$=17.5 °C and $p_{\rm atm}$=0.09927 MPa. Δp at the bottom is the range of variation for the reservoir overpressure. Pressure and temperature within the gas reservoir ($p = p_{\rm atm}+\Delta p$ and $T = T_{\rm atm}+3$) are fixed during a single simulation as the initial steady-state condition, and do not change as $p_{\rm atm}$ and $T_{\rm atm}$ evolve in time.

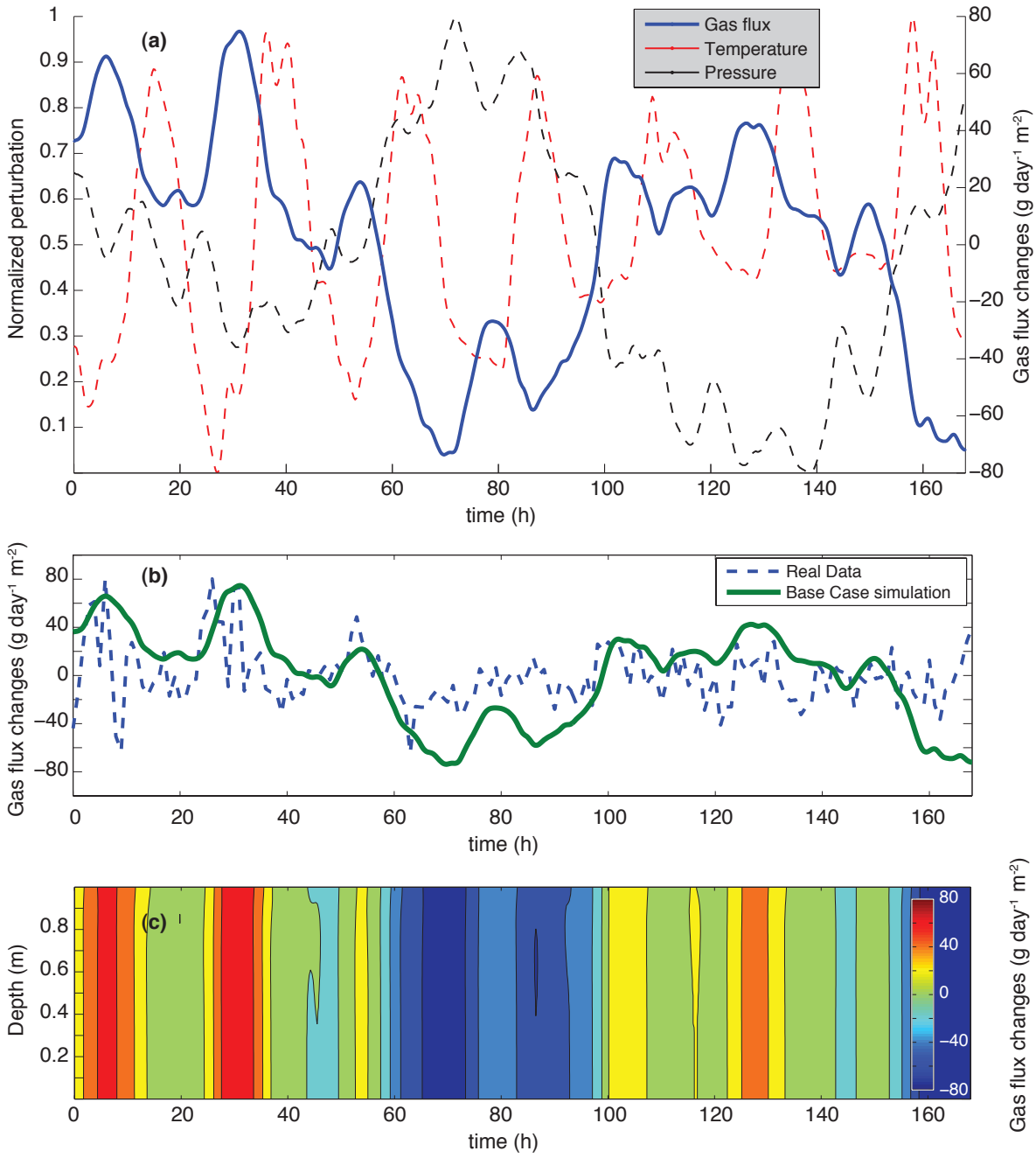

Figure 5. (**a**) Simulated temporal CO_2 flux changes (blue line) at the surface due to the application of both atmospheric pressure (black line) and temperature (red line) weekly variation. For this base case permeability $\kappa = 2 \cdot 10^{-14}$ m^2 and reservoir overpressure $\Delta p = 0.05$ MPa were considered. (**b**) Comparison with the real flux changes (blue line) observed at station GFUR2 at Furnas. (**c**) CO_2 changes in time and depth.

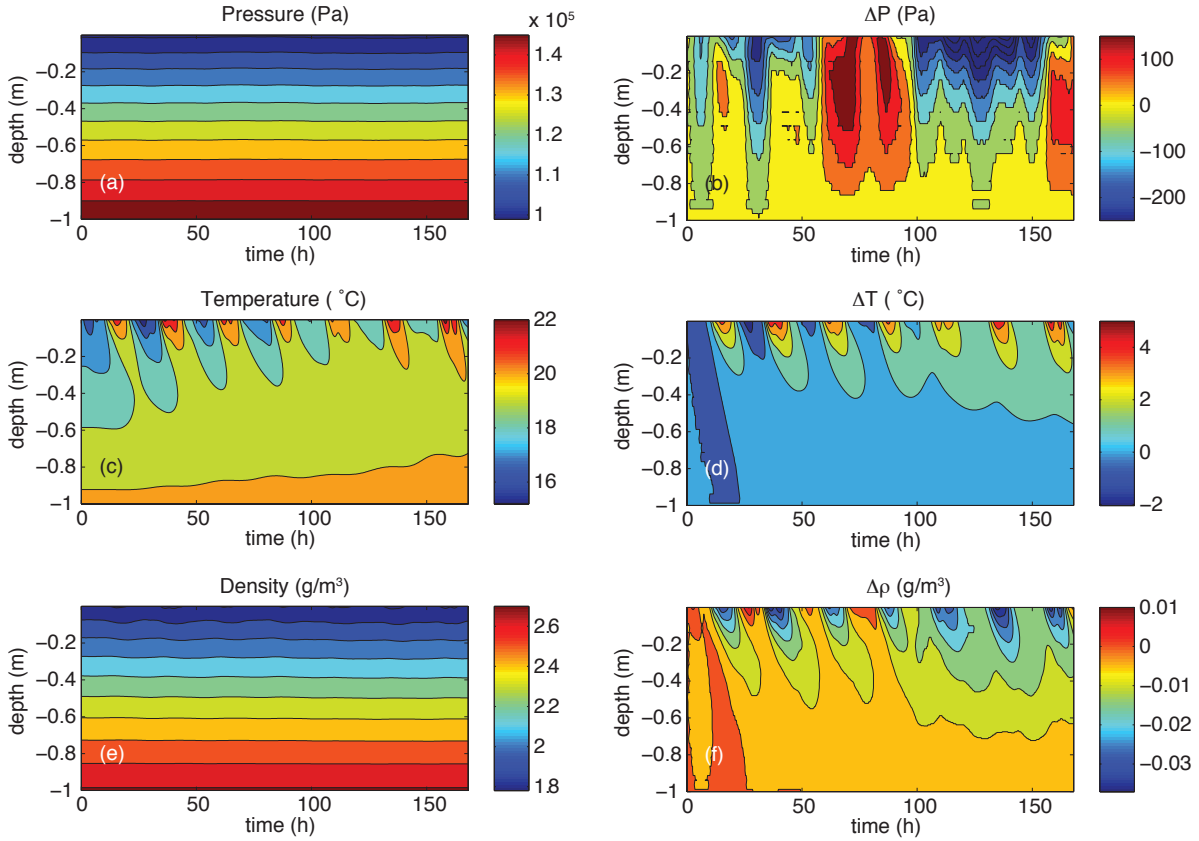

Figure 6. (**a,c,e**) Pressure, temperature and gas density in time and depth for the base case simulation. (**b,d,f**) Variation of p, T, and ρ in time and depth with respect to the initial steady state condition.

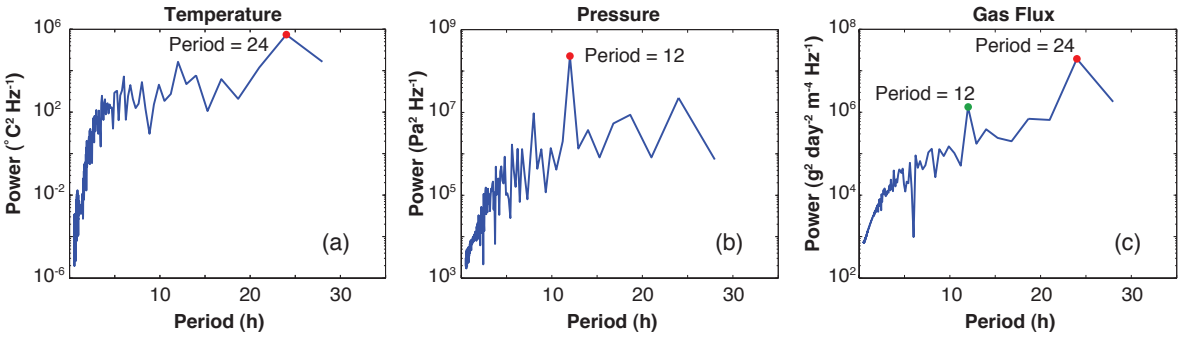

Figure 7. Low-pass filtered spectra for temperature (**a**), pressure (**b**), and simulated gas flux (**c**): all the periods larger than 28h are have been filtered. Red dot indicates the main peak for each time series.

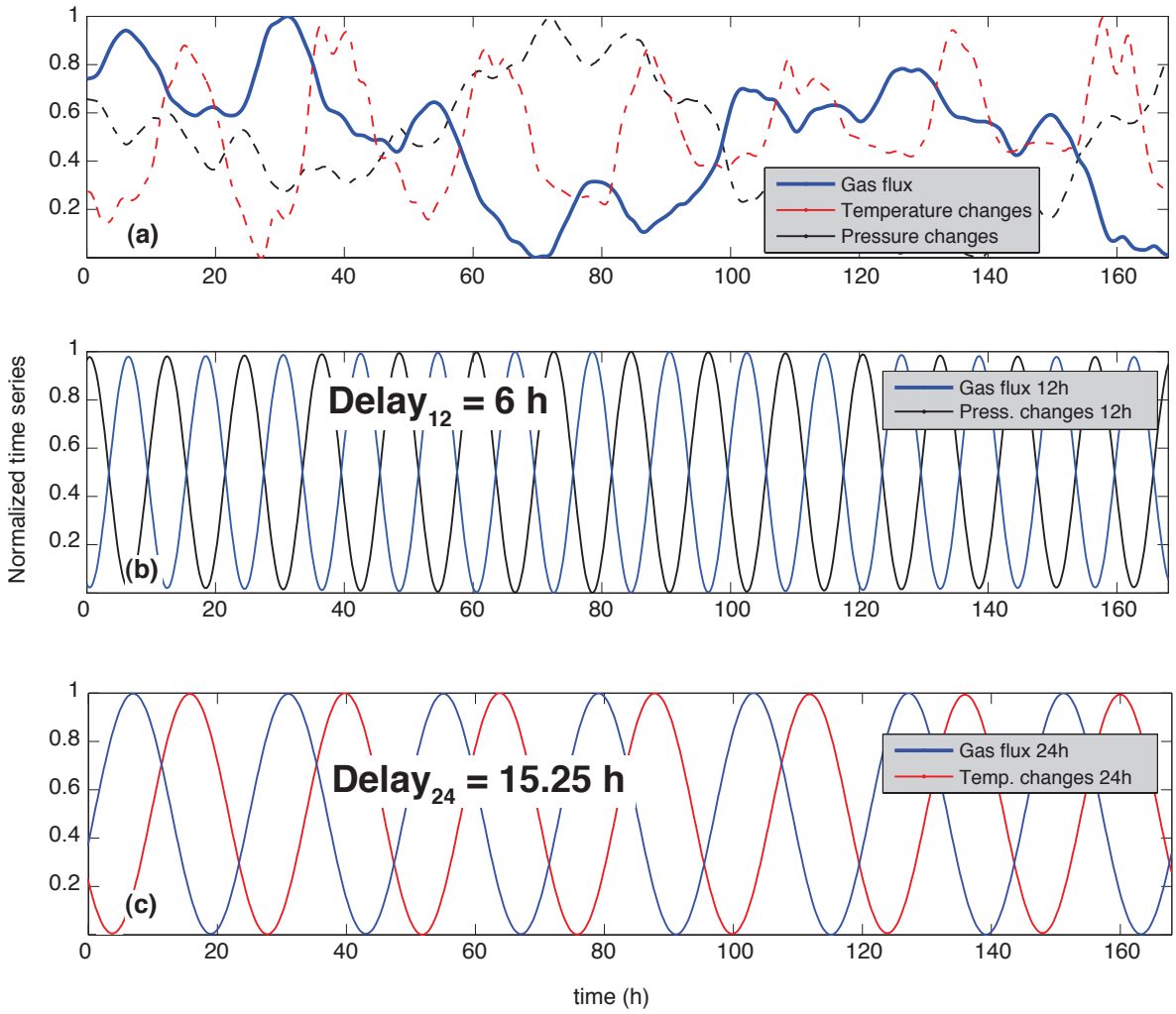

Figure 8. (**a**) Normalized time series: pressure (black), temperature (red), and simulated gas flux (blue). (**b**) Normalized and filtered time series for the 12h component: pressure (black) and simulated gas flux (blue). CO_2 flux is 6 hours delayed with respect to the pressure time series. (**c**) Normalized and filtered time series for the 24h component: temperature (black) and simulated gas flux (blue). CO_2 flux is 15.25 hours delayed with respect to the temperature time series.

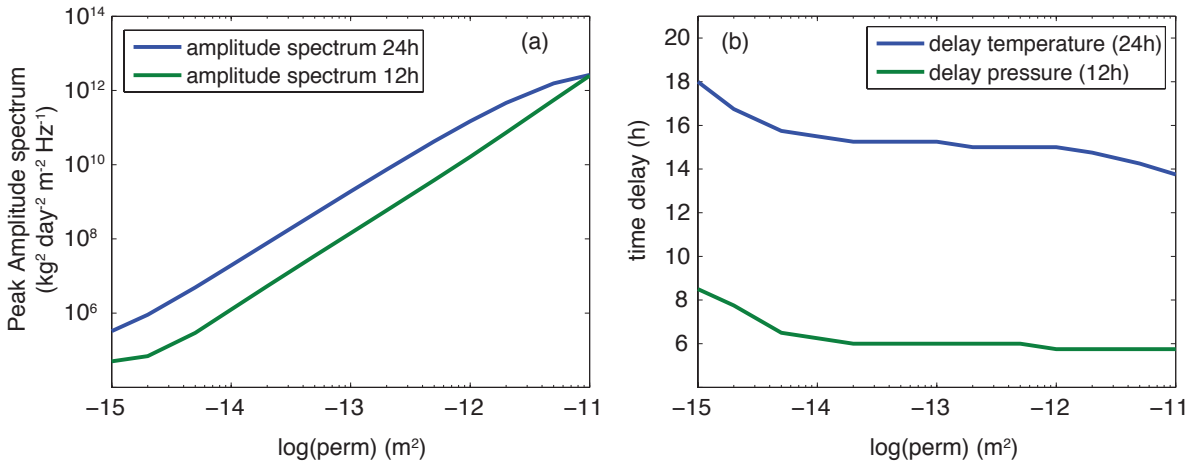

Figure 9. (**a**) Peak amplitude in the spectrum of the CO_2 flux as a function of the domain permeability for the 12h (green line) and 24h (blue line) component, respectively. (**b**) Time delay as a function of the domain permeability, with respect the pressure (12h component, green line) and temperature (24h component, blue line), respectively. For this set of simulations reservoir overpressure was fixed as in the base case (0.05 MPa).

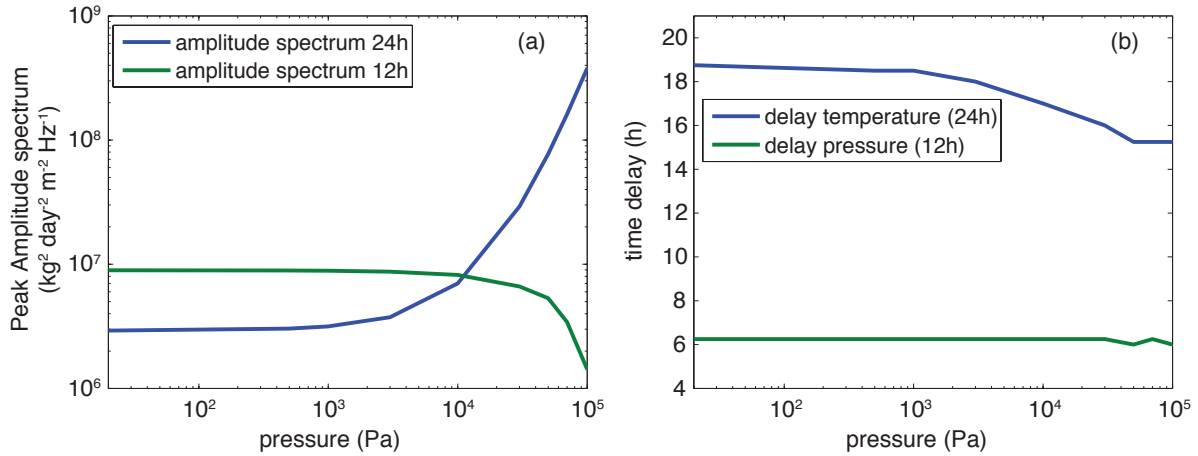

Figure 10. (**a**) Peak amplitude in the spectrum of the CO_2 flux as a function of the reservoir overpressure for the 12h (green line) and 24h (blue line) component, respectively. (**b**) Time delay as a function of the reservoir overpressure, with respect the pressure (12h component, green line) and temperature (24h component, blue line), respectively. For this set of simulations domain permeability was fixed as in the base case ($2{\cdot}10^{-14}$ m^2).

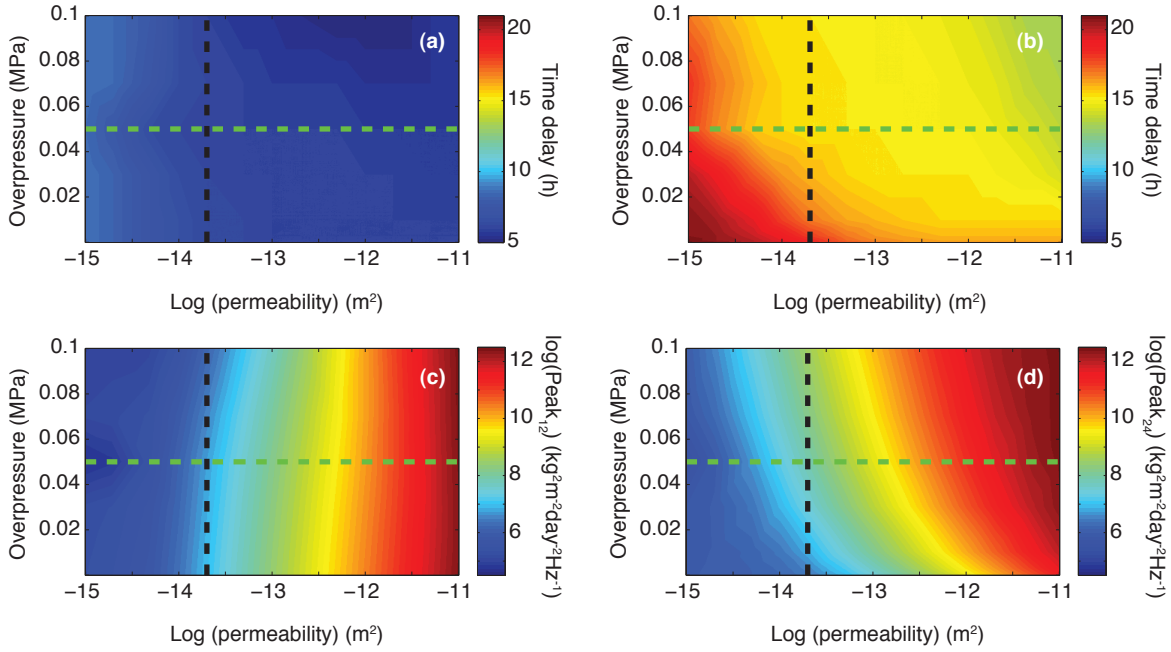

Figure 11. Dual parameter study: time delays and peak amplitudes of the CO_2 gas flux as a function of both gas reservoir overpressure and rock permeability. (**a**) Time delay of the 12h component with respect to the barometric pressure. (**b**) Time delay of the 24h component with respect to the air temperature. (**c**) Peak amplitude of the 12h component. (**d**) Peak amplitude of the 24h component. Black and green line represents in all figures the value used previously for the analysis of the degassing as a function of only the rock permeability or gas reservoir overpressure, respectively.

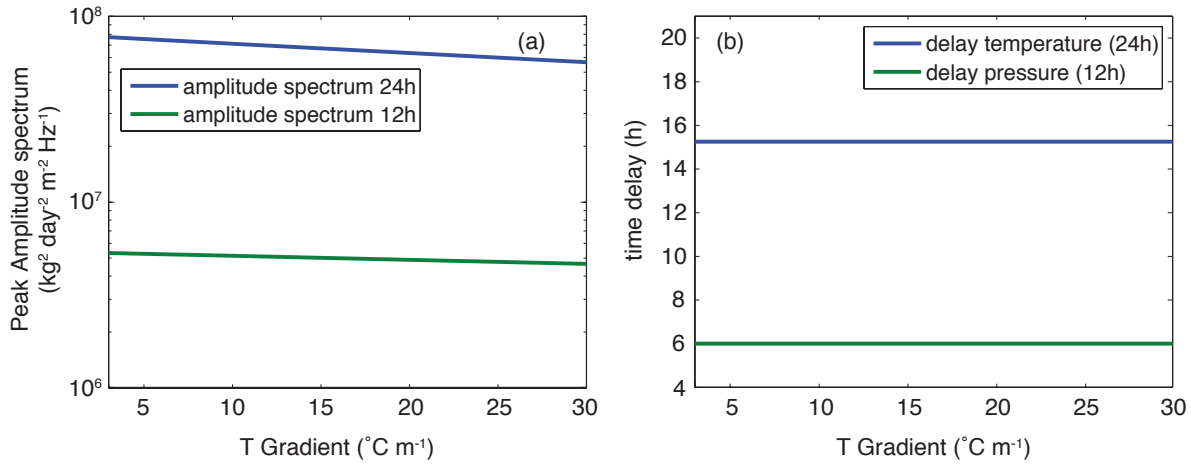

Figure 12. (**a**) Peak amplitude in the spectrum of the CO_2 flux as a function of the temperature gradient for the 12h (green line) and 24h (blue line) component, respectively. (**b**) Time delay as a function of the temperature, with respect the pressure (12h component, green line) and temperature (24h component, blue line), respectively. For this set of simulations domain permeability and gas reservoir overpressure were fixed as in the base case ($2{\cdot}10^{-14}$ m^2, and 0.05 MPa, respectively).